Journal of Biomedical Informatics 79 (2018) 117–128

Contents lists available at ScienceDirect

Journal of Biomedical Informatics

journal homepage: www.elsevier.com/locate/yjbin

Computer-Assisted Decision Support System in Pulmonary Cancer detection and stage classification on CT images

Anum Masood[a,b], Bin Sheng[a,*], Ping Li[c], Xuhong Hou[d], Xiaoer Wei[d], Jing Qin[e], Dagan Feng[f]

[a] Dept. of Computer Science and Engineering, Shanghai Jiao Tong University, China
[b] Dept. of Computer Science, COMSATS Institute of Information Technology, Pakistan
[c] Faculty of Information Technology, Macau University of Science and Technology, Macau
[d] Shanghai Jiao Tong University Affiliated Sixth People's Hospital, China
[e] School of Nursing, The Hong Kong Polytechnic University, Hong Kong
[f] School of Information Technologies, The University of Sydney, Australia

ARTICLE INFO

Keywords:
Lung cancer stages
Nodule detection
Deep learning
Convolutional neural networks (CNN)
mIoT (medical Internet of Things)
MBAN (Medical Body Area Network)

ABSTRACT

Pulmonary cancer is considered as one of the major causes of death worldwide. For the detection of lung cancer, computer-assisted diagnosis (CADx) systems have been designed. Internet-of-Things (IoT) has enabled ubiquitous internet access to biomedical datasets and techniques; in result, the progress in CADx is significant. Unlike the conventional CADx, deep learning techniques have the basic advantage of an automatic exploitation feature as they have the ability to learn mid and high level image representations. We proposed a Computer-Assisted Decision Support System in Pulmonary Cancer by using the novel deep learning based model and metastasis information obtained from MBAN (Medical Body Area Network). The proposed model, DFCNet, is based on the deep fully convolutional neural network (FCNN) which is used for classification of each detected pulmonary nodule into four lung cancer stages. The performance of proposed work is evaluated on different datasets with varying scan conditions. Comparison of proposed classifier is done with the existing CNN techniques. Overall accuracy of CNN and DFCNet was 77.6% and 84.58%, respectively. Experimental results illustrate the effectiveness of proposed method for the detection and classification of lung cancer nodules. These results demonstrate the potential for the proposed technique in helping the radiologists in improving nodule detection accuracy with efficiency.

1. Introduction

Ubiquitous internet access has opened the door for the biomedical researchers to obtain the dataset as well as the latest techniques available online and use them for developing improved health care-systems. Health-related Internet of Things (H-IoT) [1] is advancing by each passing day and innovative ideas are surfacing more frequently, targeting the health sector especially the detection and diagnosis of disease. Recently the advancements in IoT technology have made it a popular multidisciplinary research topic both in academia and industry particularly in healthcare sector [2–4]. Previously the usage of Information and communication technologies in healthcare sector was limited and often considered as a risk but nowadays ICT is offering promising medical services to patients, mostly referred to as e-health which includes electronic record systems [5], personalised devices for diagnosis, etc. Traditional healthcare systems are frequently being replaced by the coherent and ubiquitous ICT enabled solutions mainly because they are able to deliver high quality patient-centred healthcare services. Rapid proliferation of smartphones and wearable devices based on IoT enabled technology [6,7] are evolving healthcare from conventional system towards personalised healthcare system. Successful utilisation of IoT enabled technology in (H-IoT) will enable efficient and reliable preventive care, low cost, enhanced patient-related practice and improved sustainability [8,9].

Pulmonary cancer (commonly known as lung cancer) is one of the most aggressive cancerous disease which results in mortality of over 70%, roughly one quarter of the deaths caused by all types of cancers. Pulmonary cancer is considered to be difficult to cure as the early diagnosis is crucial to save the patient. Most of the lung cancer patients are diagnosed when the disease is at an advanced stage. However, an early detection of pulmonary cancer could increase the chances of cure. Detection of pulmonary cancer in early stages is difficult mainly because there is lesion growth which is of dime-size within the lung called nodule. The first step towards the cure of lung cancer is detection of

* Corresponding author at: Department of Computer Science and Engineering, Shanghai Jiao Tong University, Shanghai 200240, China.
E-mail address: shengbin@sjtu.edu.cn (B. Sheng).

https://doi.org/10.1016/j.jbi.2018.01.005
Received 23 June 2017; Received in revised form 12 December 2017; Accepted 15 January 2018
Available online 31 January 2018
1532-0464/

lung nodules in its early stage thus the treatment could be started before it becomes malignant. Conventional method for detection of lung cancer is mass screening process by using X-ray films. Small lung cancer nodules are not easily detected using X-ray at early stage because of organ's shadow and the bone's overlapping. Therefore, these lung nodules remain undetected by X-rays and are detected only by Computerized Tomography (CT) Scan. CT-Scan revolutionized medical image processing by presenting 3D imaging. In the beginning CT-Scan slices were obtained and reconstructed to be further imaged on film. Recent CT scanners are able to reformat this large amount of volumetric data in various planes as well as visualize using high resolution volumetric (3D) representations. These technological innovations improved lung cancer detection and diagnosis, using CT images, by the help of various computer assisted detection systems (CADe). With the advancement in the field of internet-of-things (IoT) [10], the medical imaging equipment is also accessible through remote sensors over the internet. The remote connectivity of these CT-Scan imaging devices has enabled the health sector to introduce new methods for the diagnosis and detection of lung cancer.

Internet of Things technology used in the field of healthcare is often termed as medical Internet of Things (mIoT). To address the challenges encountered in medical and health care information, mIoT provides advantages in the recording of patient data, its analysis and use of acquired information for diagnosis [11]. Revolution in mIoT is redesigning health care sector with promising state-of-the-art IoT-based health care solutions [12]. With the use of IoT-based health care methods, the diagnostic and monitoring functions performed by physicians today can be offset to computation methods and algorithms. Improvement in diagnostic accuracy by physicians could likely be assisted by use of different deep learning models [13]. In case of pulmonary cancer, the follow-up check-ups of the patients are mandatory. These follow-up check-ups comprised of CT-Scan of the patient and the physiological information. Deep learning model are trained using these CT image data to get the characteristics of pulmonary cancer nodules, and then screen the images for nodules using the trained model. The obtained results are provided to the radiologists to make a decision for the diagnosis of the patient [14,15]. The conventional diagnosis process is time consuming as the radiologist marks the location of the lung nodule on the other hand the automation of this nodule detection using different computer assisted detection (CADe) tools enable fast diagnosis with higher accuracy. The radiologists use CADe as a second opinion for decision on the pulmonary cancer stage diagnosis.

Our proposed technique is based on the deep fully convolutional neural network (FCNN) for initial classification into normal CT-Scan image and patient's CT-Scan image. Nodules are detected by using the pre-processed input images for the training of the deep FCNN. Afterwards each detected nodule is classified into four cancer stage based on the malignancy of the detected nodule and the metastasis information recorded by using various sensors. The performance of proposed work is evaluated on six different datasets with heterogeneous scan parameters. The performance of proposed technique was evaluated by comparing the results with the existing state-of-the-art CNN technique TumorNet [16]. Experimental results showed that the proposed technique can be used for the detection as well as classification of lung cancer nodules. Section 2 describes the related work. Section 3 presents the proposed method in detail and based on experimental results (Section 4), the conclusion is presented in Section 5.

2. Related work

Recent researches have shown that deep neural networks have great potential for CAD application involving volumetric medical data [17]. Few of these studies have used neural networks for detection and diagnosis of pulmonary nodules [18], among which ensemble methods using neural networks have shown the best results [19]. Artificial Neural Networks (ANN) method is also used for the nodule detection [20,21]. This research work was based on the difference-image technique in which the pulmonary nodules were enhanced and the normal background structures were suppressed. Afterwards thresholding technique was applied and lastly the nodule candidates' image features were quantified. Rule-based method and ANN were used simultaneously to eliminate the FP results.

Feed forward NN was also used by [22] for classify nodules in X-ray images with limited features such as shape, perimeter and area. In recent years, convolutional neural network (CNN) has become a benchmark in the field of CADx systems. CNN is used to detect lung nodule and the results are promising [23]. There are two main methods of using CNN, either the researcher can model their own CNN architecture or they can use off-the-shelf CNN for acquiring the features [24]. DFCNet takes classification to a whole new level, using the dense prediction by considering the convolution nets as fully convolutional and fine-tuning is done in such a way that the predecessor layer sends the learned features to the current convolution layer. FCNN are different from the existing CNN [25] as they only used small convolutional network and the learned features were not used as pre-training by the successor layer [26]. In our research work we used fully convolutional NN not only for detection of the nodule but also for the classification of the lung cancer stage.

3. Proposed approach

The Internet of Things (IoT) refers to use of sensors that can transmit the gathered information over the internet. For computer-assisted decision support system in pulmonary cancer detection we used four main steps: data recording using sensors and CT-Scan Images, collection of obtained dataset over the internet, training the model using the obtained dataset and diagnosis decision making based on trained model as shown in Fig. 1. This decision is further provided to the radiologists for assisting them in improved diagnosis decision for pulmonary cancer stage classification. Pulmonary cancer has four stages. Stage-1 nodule size is smaller in size about > 3 mm and $\leqslant 20$ mm is restricted to the lungs. The nodule size of Stage-2 pulmonary cancer is within the range of 21–30 mm and is spread to surrounding lymph nodes. Stage-1 and Stage-2 are early stages of cancer. In Stage-3, the cancerous cells are extended to other nearby organs and the size of nodule is approximately between 30 mm and 70 mm. In the last stage (Stage-4) of pulmonary cancer, the nodule size is more than 70 mm and is spread outside the lungs to other vital organs of body. Stage-3 and Stage-4 are often referred to as advance Stages of cancer.

For the first step of our computer-assisted diagnosis (CADx) system, the sensors attached to patient's body forming body area network (BAN) which collects comprehensive physiological information and uses gateways to forward that data to network (see Figs. 2–4).

Physiological symptoms of patients can be constantly monitored remotely using wearable IoT device. Depending on the stage of pulmonary cancer, symptoms of lung cancer differs [27]. Pulmonary cancer symptoms are mostly visible when the cancerous cells are spread out in the body. In some cases, early stages (Stage 1 and 2) also have symptoms. Most common symptoms for early stages of pulmonary cancer are chest pain; cough, rust-colored spit (phlegm), body-weight loss, breathlessness, fatigue, infections (pneumonia/bronchitis), wheezing, difficulty in swallowing, and swelling of feet [28].

In case, there are malignant nodules due to which the cancer is spreading to distant organs then symptoms such as backache, seizures, dizziness, numbness, yellowing of skin (if its spread to liver), appearance of lumps near body surface (neck/collarbone), blood pressure, hypercalcemia commonly known as high blood calcium levels can cause constipation, nausea, vomiting, pain, fatigue, anxiety, confusion, and various nervous system problems. These symptoms are not necessarily due to pulmonary cancer but research studies show that these can be caused by pulmonary cancer. The probabilities of occurrences of physical symptoms for different stages of Lung cancer [29] are shown in

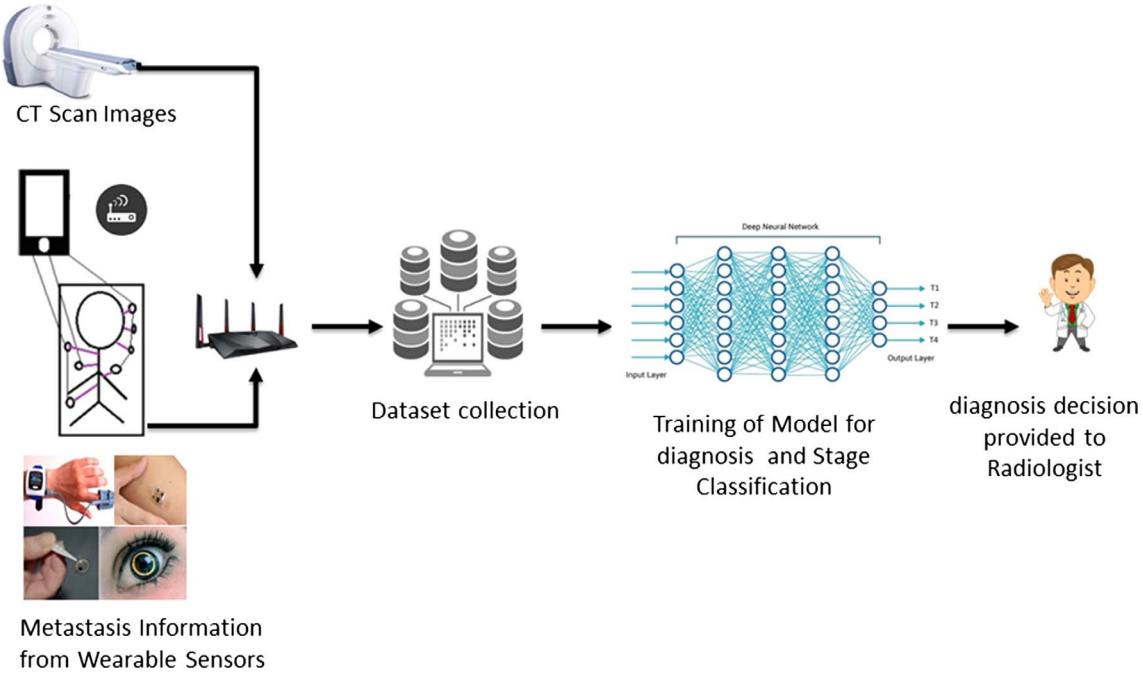

Fig. 1. Overview of the four stages of computer-assisted decision support system.

Table 1.

According to Table 1, the common symptoms for all stages are body weight loss (BWL), Breathlessness (BLN), Heart Rate (HR), High Body Temperature (HBT), Blood Pressure (BP), Insomnia (INS), Hypercalcemia (HC) which is the cause of pain, fatigue, constipation, etc. For acquiring these metastasis features for the stages classification, sensors were used. The data collection for the metastasis features was done by using the IoT based personalized health-care systems both clinical system and remote monitoring system.

Shanghai Hospital No. 6 provided the patients metastasis information (BWL, BLN, HR, HBT, BP, INS, HC) by non-invasive IoT-based sensors for gathering physiological data that was stored on a Cloud for instant updating. In few cases, remote monitoring was used to access health monitoring of patient using sensors. Multiple sensor nodes were connected to Internet which was used to gather information by remote monitoring devices [30].

This research work is targeted to find a method to assist with the early detection and stage classification of lung cancer, relieving doctor's burdens, and providing better treatment options for the patients. We proposed a Computer-Assisted Decision Support System in Pulmonary Cancer by using the deep learning model DFCNet and metastasis information obtained from MBAN (Medical Body Area Network) which are lower power network comprising of control transmitter, sensor devices worm by the patient which receives the control commands in process of measuring physiological parameters for diagnostic purposes. The recent progress in the 5G Technology will be useful in recording the real-time physiological data of each patient and its storage as well as processing [31]. Vendors such as Philips, Qualcomm are manufacturing

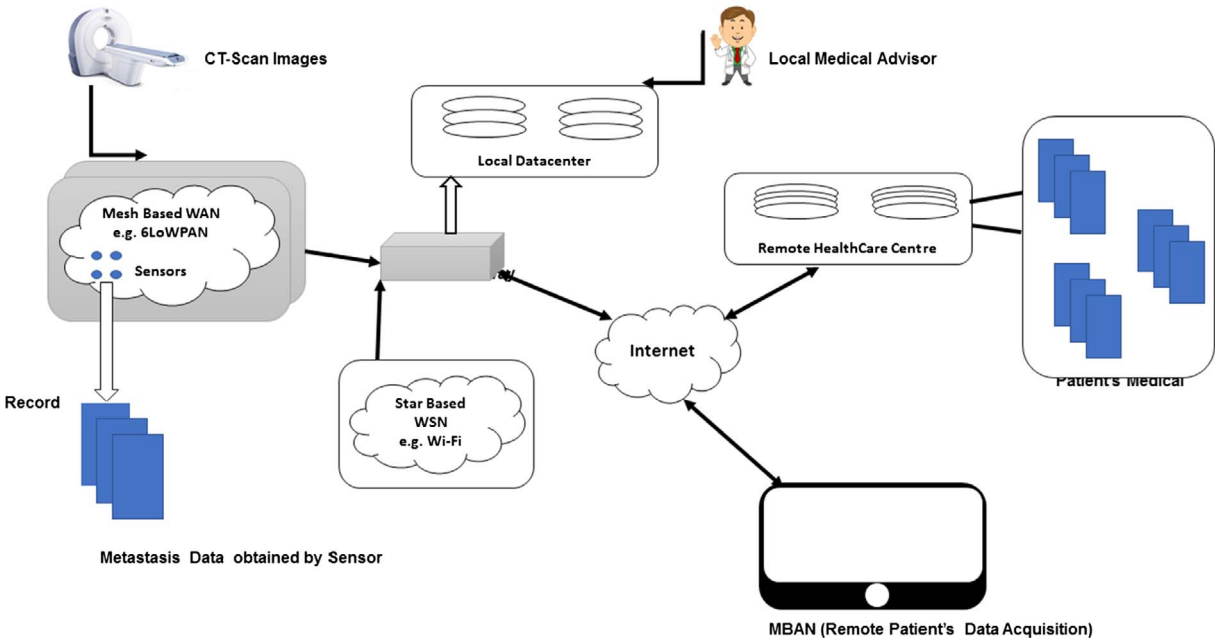

Fig. 2. Communication between the devices for computer-assisted decision support system.

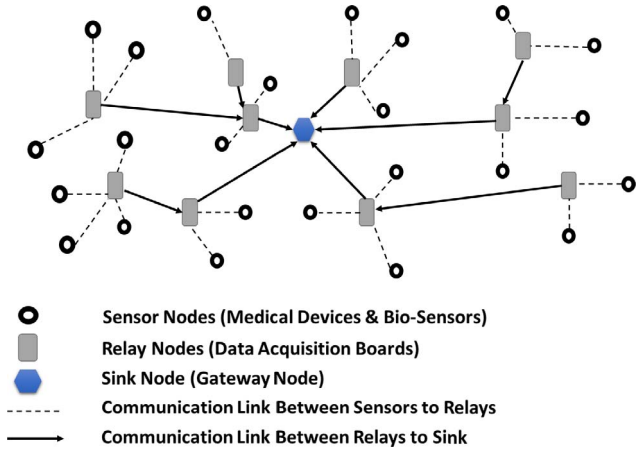

Fig. 3. Communication between the sensor nodes.

MBAN devices which are expected to send real-time physiological information of patients to physician onto their smartphones and PCs. These MBAN devices will have a specific spectrum range of 2360–2400 Hz band. This specific spectrum range ensures that other wireless devices could not interfere with MBAN transmission. It is significant that there is no interference from other wireless devices when MBAN devices are sending real-time physiological information of patients to the physicians.

Due to unavailability of such devices at the time of this research work, we mainly used sensors on the clinical healthcare centre (in our case it was Shanghai Hospital No. 6). We also used remote monitoring devices (smartphones applications) for recording the metastasis parameters. Wearable IoT (WIoT) is an infra-structure that interconnects

Table 1
Symptoms prevalence for lung cancer stages.

Symptoms	Stage 1 (%)	Stage 2 (%)	Stage 3 (%)	Stage 4 (%)
Body weight loss	35–63[1]	45–60	91–94	93–99
Breathlessness	3–55	40–87	90–95	97–99.5
Irregular heart rate	11–62	18–73	92–96	92–99
High body temperature	55–65	31–78.7	93–97	94–98
Blood pressure	29–43	63–87	89–92	90–93
Pain	27–44	29–62	34–77	41–81
Depression	18–32	22–47	37–77	46.5–83
Anxiety	36–48	44–64	61–75	80–94
Fatigue	17–38	27–44	68–80	77–88
Insomnia	38	49–61	75–88	87–91
Constipation	11–20	19–23	27–44	40–60
Anorexia	–	–	35–67	39–76

Minimum-maximum range of prevalence (%).

wearable technology to exchange data with wearable sensors and to send data to cloud. Bluetooth is used for exchanging data with sensors whereas WIFI is used to send the recorded data to Cloud for further processing.

For our proposed work, we used monitoring devices both in form of wearable devices and smartphone applications. Information for insomnia parameter was gathered by recording the sleeping-pattern by the help of MI-Band (wearable device). Breathlessness physiological information was obtained by recording the respiratory rate/breathing index using Rejuven's Rejiva. Heart Rate was obtained by using the smartphone applications named Runtastic heart rate/Instant heart rate application. Body Temperature was recorded by the help of a smartphone application Finger print thermometer. Blood Pressure was acquired using wearable BP sensor and body weight loss by health assistant application.

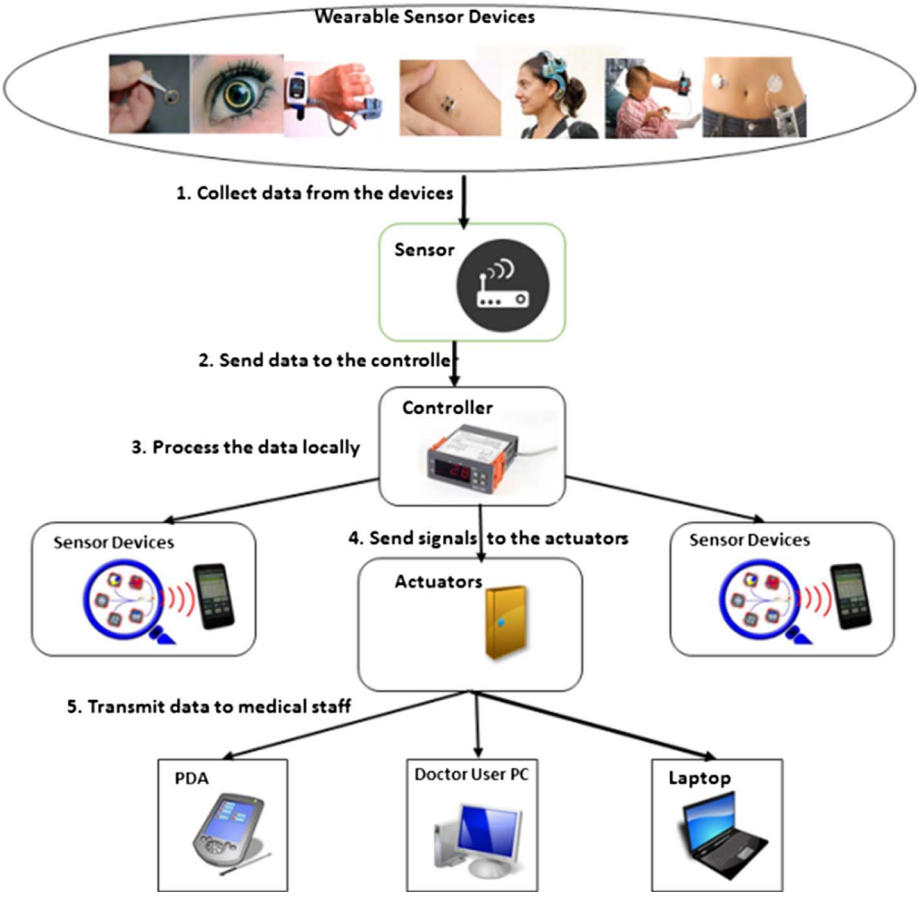

Fig. 4. Communication among wearable devices.

Although the remote monitoring devices are more convenient yet they are not accessible to all patients therefore for the stage classification we used the data collected by the clinical healthcare system. The benefit of connecting these sensors with cloud is to use Electronic health records (EHRs) for further training of the FCNN model. Different datasets was used for training of the proposed work. The dataset was from 6 different sources LIDC-IDRI database [32], RIDER [33], LungCT-Diagnosis [34], and LUng Nodule Analysis (LUNA) 2016 Dataset [35]. These are publicly available in the The Cancer Imaging Archive (TCIA) [36], and the pulmonary nodules have been fully annotated by multiple radiologists. Radiologists manually segmented the lung nodules with size of 3 mm or more.

For the variations in the lung CT images, we used the LISS database which comprises of 9 different categories of CT imaging signs of lung diseases. These imaging signs are detected and labelled (region labelling and class labelling) by the radiologists [37]. LISS database comprises of 271 Lung CT scans while 677 abnormal regions in these CT Scans which are sub-divided into nine classes (Lobulation *L*, Calcification *C*, Cavity and Vacuolus *CV*, Spiculation *S*, Plueral Indentation *PI*, Air Brochogram *AB*, Bronchial Mucus Plugs *BMP*, Obstructive Pnemonia *OP*, Grand Grass Opacity *GGO*) of CT imaging signs of pulmonary disease. For the DFCNet training, the CT-Scans of all the classes were used. Table 2, shows the details of each class of LISS dataset for training along with its indication in terms of malignancy in the nodule.

Radiologists have stated that more than one type of class can exist in a single nodule therefore they have to consider all the signs and predict whether the nodule is benign or malignant. The same idea is considered here to train the DFCNet using different samples of these classes and predict the malignancy of the nodule in given CT-Scan. There was another dataset that was not used in training phase, SPIE Challenge Dataset [38], which was not annotated in order to test whether the DFCNet is able to detect nodule and non-nodule without annotations. There was information about location on the largest cross-sectional area of nodule CT-Scan which was only used for extracting the CT-Scan slices and pre-processing of these images was necessary. The workflow of the proposed work is shown in Fig. 5.

The input of the DFCNet was originally $512 * 512$ slices with one colour channel (grey level 0–255). In order to prepare the desired input of $100 * 100 * 3$, all of the images were resized to attain the $100 * 100$ size. The grey level channel was duplicated into two other colour channels to provide the 3 required colour channels to the DFCNet pre-trained convolution layer (see Fig. 6).

3.1. Pre-processing

Various filters could be used for enhancing the images. We used low-computational Gabor filter [39] for the enhancement of the CT-Scan images before using these CT-Scan images for segmentation of region of interest.

3.1.1. Lung Region-of-Interest Extraction using the thresholding method

Thresholding is the most commonly used technique for Region-of-Interest (ROI) Extraction. In this technique, the object-background is selected and then threshold is obtained which divides the image pixels into either object or background. In this way, the ROI is extracted from the background and which is used for the training of the DFCNet. DFCNet detects whether the given voxel is likely to be a nodule or not, based on the spatio-temporal statistics around it. A nodule can range from 3 to 28 pixels wide at its largest size, and spans 3–7 slices typically. For every nodule 48 unique perspectives were selected, which enlarged the initial dataset by 48 times. Furthermore, random crop of image slices was done for each slice which resulted in increasing the dataset, for instance the initial dataset of 932 pulmonary nodules of LIDC-IDR was increased to 465,504 training image-slices.

Table 2
Nine classes of LISS database for training of DFCNet.

LISS database classes [37]	Total number of CT-Scans	Training CT-Scans	Testing CT-Scans	Sign of malignant or benign nodule
GGO	25	17	8	Malignant
L	21	14	7	Malignant
CV	75	52	23	Malignant
PI	26	17	9	Malignant
AB	22	19	7	Both
C	20	15	5	Both
OP	16	11	5	Both
BMP	29	20	9	Benign

3.2. Deep neural network architecture

Convolutional neural networks are advance version of the multilayer perceptron architecture and designed specifically for 2D structure image Use of tied weights as well as local connections across the layers of a CNN results in producing invariant features. Basic architecture of CNN comprises of multiple convolutional and subsampling layers at fully connected layer. Input image I having dimensions $n \times n \times Ch$ (height × width × channels, i.e. $Ch_I = 1$ (grey scale 0–255)). Within a convolutional layer of CNN, there are filters K of size $m \times m \times Ch_F$, where $m < n$ and $Ch_F \leqslant Ch_I$. The kernel convolution and input image I generated features F of size $n-m+1$. For subsampling of each map, there is a pooling layer $p \times p$ $(2 \leqslant p \leqslant 5)$ which uses mean and max values.

3.3. Implementation details

For the initial implementation of DFCNet, the CT-Scan images of 18 patients were collected from Shanghai Hospital No. 6. These CT-Scan images were annotated and the nodules were segmented manually by the radiologist. Out of these 18 images, 11 were used for training of CNN whereas 7 were used for testing.

CT-scan images were patch-wise analysed for training of CNN afterwards subsampling process analysed extracted image patches for obtaining the ROI (region-of-interest). These sampled patches were used for training CNN. The size of each patch J was 32×32, which was enough for extracting meaningful information from J. Large size patches are avoided as they can contain unnecessary information and therefore increase the complexity.

The CNN architecture comprises of 7 convolution with Parametric ReLU Rectified Linear Units (PReLU) [40] with $\alpha = 0.25$, 7 max-pooling layers ($Mpool_n$ $n = 1,...,7$), 7 batch normalization layers ($Bnorm_n$ $n = 1,...,7$), and two dense layers $Conv_{2048}$ with Leaky Rectified Linear Units (LreLU) with $\alpha = 0.01$, a final 1000-dimensional dense layer, deconvolutional layer $Deconv_8$ with a Softmax classifier (large margin softmax loss) on top. If the value of α is fixed and small then the PreLU used with convolutional layers will become the Leaky ReLU (LreLU) in [41]. The main purpose of using LreLU is to avoid zero gradients. All convolutional layers ($Conv_{64}$,$Conv_{128}$,$Conv_{256}$) use 3×3 sized filters with stride of 1 except for the last three convolutional layers. The first $Conv_{4096}$ uses filter size of 7 while the other $Conv_{4096}$ and $Conv_2$ uses filter size 1. As these convolutional layers follow the pattern of linear layers applied to pixels of input image I therefore they enable the NN to be fully convolutional. $Conv_2$ assigns a score for both of the classes for each given pixel. Max-pooling is performed using the window of size 2×2 with stride of 2. The deconvolutional layer $Deconv_8$ uses filter size of 16 with a stride 8. Afterwards resultant image is centre-cropped to $2 \times 128 \times 128$ before the softmax layer. Dropout regularization was done using dropout 25% on the convolutional layers ($Conv_{64}$,$Conv_{128}$,$Conv_{256}$) while dropout 50% for both $Conv_{4096}$

Convolutional layer considers the local regions of I and the neurons connected to this region to obtain the output. The set of learnable filters were the basic parameters for the convolutional layer. After each

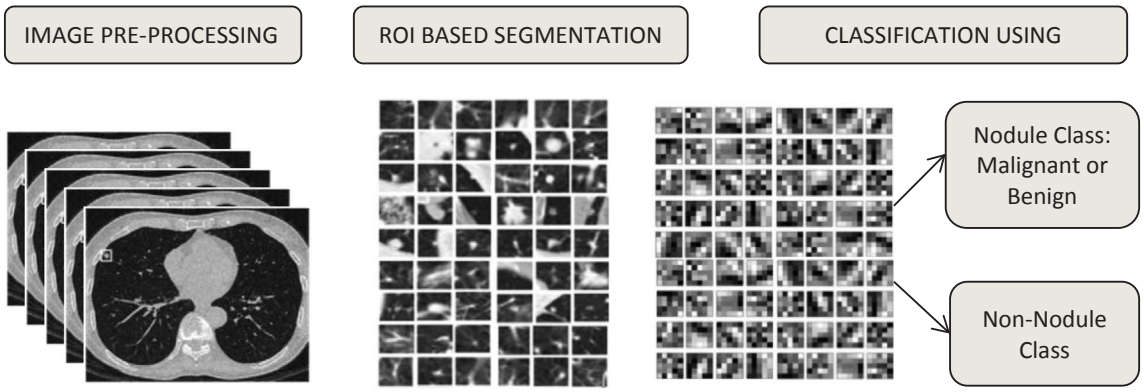

Fig. 5. Pipeline of proposed work consisting of three prominent phases: (a) Pre-processing, (b) deep neural network, and (c) classification.

forward pass, filter's 2D activation map is generated by sliding filter over the input volume. This is repeated to obtain the complete output volume. There are few hyperparameters required by each layer; filters K, stride S, receiver field R, spatial dimensions D and zero padding Z. The output volume can be calculated as:

$$W_O(D) = 1 + \frac{W_I(D) - R + 2Z)}{S} \tag{1}$$

All convolutional layer use zero padding $P = 1$, except for the first layer, which uses zero padding of 11 to avoid reduction of size after the max-pooling phase. Down-sampling along the spatial dimensions d is done in the pooling layer. Pooling layer uses *max* operation and resizes each input slice spatially. Pooling layer required volume of input (weight, height, depth) $w_I \times h_I \times d_I$ and other hyperparameters such as stride S, receiver field R, spatial dimensions D. The purpose of pooling layer within the network is avoiding over-fitting, parameters reduction and overall fast computation of DFCNet.

Last layer output is linked to the softmax layer which distributes the given input into two classes (nodule and non-nodule). Softmax function is applied to all the pixels one by one. For each given pixel, softmax function assigns two scores, one for each class (nodule and non-nodule) to provide class probabilities (p_n and p_{non}). These class probabilities (p_n and p_{non}) are transferred to the large-margin loss layer [42]. In other words, this layer is a combination of softmax layer followed by the large margin softmax loss layer. DFCNet was trained for 50,000 steps, with 16,384 members (128 × 128 pixels) per mini-batch. The performance of DFCNet depends on the network hyperparameters initialization. As these hyperparameters are initialized randomly therefore the performance can vary even if these hyperparameters are exactly the same. In order to avoid this wide variation in the performance with same hyperparameter, the model is trained multiple times with same hyperparameters to obtain the optimized performance and normalize the input image I to each layer using the batch normalization technique. Batch Normalization [43] was applied to convolutional layer of the network. The normalized activations $\hat{a}$ distribution mean value is expected to be 0 while the variance is expected to be 1. Once the DFCNet has been trained, we use the normalization function:

$$\hat{a} = \frac{a - E[a]}{\sqrt{Var[a] + \epsilon}} \tag{2}$$

If ϵ is neglected in the training of DFCNet then the normalized activations $\hat{a}$ has variance 1 and mean value of 0. The unbiased variance estimate could be used as, $Var[a] = \frac{b}{b-1} \cdot E_b[\sigma_b^2]$, where the mini-batch size of b is over-trained and the sample variances are represented as σ_b^2. During the training, the means and variances are fixed therefore we can consider the batch-normalization as a linear transform which is applied to each activation step.

In the large margin loss layer had a total loss equal to the average loss per pixel in I. Since the size of the nodule is 3 mm or above, therefore it comprises of approximately 2.5% of the input image I pixels. Therefore, in the loss L equation, the nodule pixels are considered to be 0.975 and the non-nodule is considered to be 0.025. For improving the performance on the testing dataset, the regularization weight of was used.

$$L_i = \left[0.975 \sum_{i=n} L_i\right]\left[0.025 \sum_{j=non} L_j\right] + w_{reg} \tag{3}$$

For the given pixel (i) of image I, the loss will be 0 (non-nodule Class C_{non}) or 1 (nodule Class C_n). The equation $L_I = -\log\left(\frac{e^{\|f_i\| \|x_i\| \theta_{f_i}}}{e^{\|f_i\| \|x_i\| \theta_{f_i}} + \sum_{j\{0,1\}} e^{\|f_j\| \|x_i\| \cos\theta_{f_j}}}\right)$ gives the score for each class for

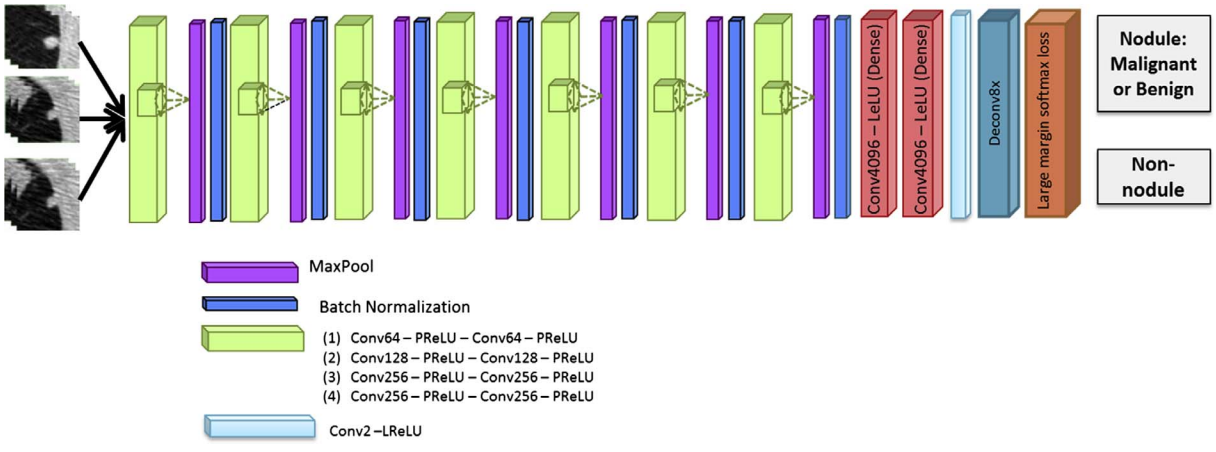

Fig. 6. Net architecture of DFCNet.

given pixel.

3.4. Learning

Any model using Batch Normalization can be optimized either by using the Stochastic Gradient Descent (SGD), or batch gradient descent (BGD) with a mini-batch size $b > 1$ [44]. Normally SGD works better when the training data does not contain many subjects. For the lung nodule dataset, the SGD was used momentum of 0.9. Each convolutional layer was initiated by the weights proposed by Long et al. [26]. For each pixel of input image I, the weights can be considered as feature set generating method which is used by the DFCNet for learning the features to do classification. The mini batch size b was considered to be 128×128. The learning rate λ was $1e-4$, and ADAM update rule with learning rate of $1e-6$ is switched when the error plateaus. Weight decay regularization w_{reg} of 0.0005. $Deconv_8$ was initialized with bilinear interpolation weights. The learning rate λ for deconvolutional layer $Deconv_8$ was 0. Equal number of positive (containing nodule) and negative datasets (containing no nodule) for each batch were used to train the DFCNet in the training step. Random selection of the positive (containing nodule) half and negative half datasets (containing no nodule) was done for each batch samples. These datasets were shuffled prior to each of the SGD iteration in order to ensure that there is no overfitting case. The DFCNet is trained to get the probability of an image belongs to nodule or non-nodule class. As there are multiple CT-Scan slices belonging to a single patient therefore the adjacency rejection method is used to minimize the repetitive nodule detection and maximize the probability of detection. Each network was trained for 50,000 iterations which are equal to approximately 120 epochs of our training dataset.

During the training phase, the batch normalization is applied to the network after convolutional or dense layers i.e. before the non-linearity while in the testing phase the batch normalization is applied to the network using a pre-defined sample mean and variance. During the training process for the nodule and non-nodule classification, this problem occurred. The reason being random hyperparameter initialization, the validation accuracy of our model was reduced. Later by adding batch normalization layers after each convolutional layer, this issue was mitigated.

3.5. Data augmentation

Data Augmentation is a technique which is used to overcome the limitation of dataset overfitting. Due to limited training dataset labelled by radiologists, nodule classification step of DFCNet was compromised. To improve the classification of nodule, data augmentation techniques such as rotation about a fixed angle, random translation, spatial deformation of the training dataset was done in order to mitigate the problem of limited labelled dataset. DFCNet further used the enriched training dataset. With enhanced dataset, DFCNet was well-trained on the data features and learning parameters. The main reason behind using the data-augmentation techniques was to ensure the equal number of images for each class.

3.6. Classification

Image input I is classified afterwards a DFCNet uses the output image O in which nodule is detected ($O \in C_n$) and then it is classified as stage of the nodule T_1,T_2,T_3 and T_4. The nodule images are fed into the DFCNet which will have four classes (T_1,T_2,T_3 and T_4), each class will provide the probability score for each input. During the testing phase, priority ranking technique is used to assign input image patch (voxel) to one of the four categories on the basis of its classification scores from each class. DFCNet assigns probability to each image patch for each of the four cancer stages (Stage T_1,Stage T_2,Stage T_3 and Stage T_4), respectively indicated by p_{T_1},p_{T_2},p_{T_3} and p_{T_4}. The probability of these four stages is a combination of average diameter, diameter range; morphological features such as volume, density, perimeter, area, energy, homogeneity (sphericity, texture); high level imaging signs of GGO, L, CV, PI, BMP, C, OP and AB [37]. All these features combined together to give the prediction score for four stages of lung cancer (p_{T_1},p_{T_2},p_{T_3},p_{T_4}). Table 5 shows the details of these features for the stage classification of the nodules.

Algorithm 1 (*Priority Ranking Decision*).

Input: Classification scores from each class (T_1,T_2,T_3 and T_4)
Output: Label L_{x_I} for given pixel x_I

```
procedure PRIORITY RANKING DECISION(Score)
  if x_I ∈ C_n (Nodule Class)
    if p_T4 > = 0.5 then
      L_xI ← Stage T4
    endif
    if p_T3 > = 0.5 then
      L_xI ← Stage T3
    endif
    if p_T2 > = 0.5 then
      L_xI ← Stage T2
    endif
    if p_T1 > = 0.5 then
      L_xI ← Stage T1
    endif
  endif
endprocedure
```

Classification of nodules into different stages is done in hierarchical manner i.e. Stage T_4Stage T_3Stage T_2 and Stage T_1. The reason behind this is that the malignant stages (Stage T_4 and Stage T_3) have relatively wide range of diameter range with higher density values. If the probability of the given image patch is high for the malignant stages then the image patch (voxel) is marked as Stage T_4 nodule. If the DFCNet gives positive classification for more than one nodule stage then the ranking is done on the basis of priority. The highest priority is given to the Stage T_4 while Stage T_1 has the lowest ranking. This method improved the results of classification of nodules and overcome the problem of multiple positive classifications for one input.

3.7. Performance evaluation

In case of classification techniques, receiver operating characteristics (ROC) curves or area under the curve (AUC) are used as evaluation parameters. AUC represents the probability that the given sample image will be classified correctly. The correct classification of the nodule and non-nodule is the objective of this research work.

The basic performance evaluation metric used for this proposed work is Dice Coefficient (intersection over union). Dice score for given prediction is calculated by counting total pixels predicted as nodule both by the DFCNet and radiologists, divided by the sum of nodule pixels predicted by the DFCNet and radiologists.

$$Dice\ Score = \frac{2|P_{FCNN} \cap P_{Rad}|}{P_{FCNN} \cup P_{Rad}} \tag{4}$$

where P_{FCNN} is the set of pixels considered as the region of interest (ROI) in the prediction and P_{Rad} is the set of pixels considered as ROI in the annotation done by the expert radiologists. Dice score values ranges between 0 (no match) and 1 (perfect match). Dice score is comparatively better than the accuracy metric as the accuracy is tend to be higher for all images because of the non-nodule pixel prevalence.

The median Dice score of the nodule detection was approximately 91.34%. As there were four radiologists for the annotation of the given dataset thus the multiple-radiologist repetition was 86%. Fig. 8 shows

the comparison of the existing work with the proposed research work.

4. Experimental results

The proposed research method is evaluated using the different datasets, LIDC-IDRI database, RIDER, LungCT-Diagnosis, and Lung Nodule Analysis (LUNA) 2016 Dataset. These are publicly available in the The Cancer Imaging Archive (TCIA), and the pulmonary nodules have been fully annotated by multiple radiologists. Expert radiologists drew outlines for the lung nodules with size of 3 mm or more.

Another dataset that we used specifically for testing is SPIE Challenge Dataset which was not annotated in order to test whether the DFCNet is able to detect nodule (malignant or benign) and non-nodule without annotations. There was information about the location on the largest cross-sectional area of the nodule CT-Scan which was only used for extracting the CT-Scan slices and pre-processing of these images. SPIE-AAPM-LUNGx does not have any detailed information about the presence of nodules and thus it was considered to be real life scenario where the patient's CT Scan is to be used to detect the nodules. For the training of DFCNet, only 22 were used whereas 46 were used for testing. There was one CT Scan in which the nodule location was ambiguous therefore this particular CT-Scan was not used.

The dataset was retrospectively collected from the radiology department clinical practice Shanghai Hospital No. 6 considering the selection criteria (size to be within the range of 3–30 mm). These CT-Scan images were annotated by the radiologist and the stage of the lung cancer was diagnosed. For the training 11 CT-Scan dataset were used (10 lung cancer patient dataset and 1 healthy person dataset) while remaining 7 were used for testing. The testing dataset from Shanghai Hospital No. 6 includes 6 lung cancer patient dataset and 1 healthy person dataset.

In case of the RIDER and LungCT-Diagnosis, we used those lung CT scans which contained pulmonary nodules to evaluate the proposed method. All of the annotated pulmonary nodule segmentations are used. Pulmonary nodules' diameter ranges from 3 to 30 mm. Each lung CT scan has approximately 200 slices while each slice comprises of 512×512 pixels (size of pixel is about 0.5–0.76 mm), and the reconstruction interval is about 1–3 mm. The nodule candidates are considered as nodules or non-nodules using annotation provided by chest radiologists. The statistics of the dataset used in training and testing phase is given in Table 3.

In the first step for enhancing the images, Gabor filter was applied on the CT images. For segmentation section, the images that have passed from enhancement step, were segmented by region growing algorithm, thus lung region or (ROI) is extracted. The processes that were applied on CT lung images are shown below in Fig. 7.

After pre-processing of the CT-Scan images, the ROI are extracted and the DFCNet is trained using these lung CT image patches. The pre-processed images were fed to the DFCNet for training. Each of the dataset was divided into two parts, training dataset and testing dataset except for the SPIE Challenge dataset as there was no annotation provided. The overall accuracy, sensitivity, specificity and false positive (FP) rate were calculated both for the existing CNN approach and the proposed DFCNet method. There false positive results were observed in the classification due to the airways and the blood vessels which appear to be a nodule during local observations. In order to reduce the false positive (FP) detection, we used an elimination method [45]. This method considers the detected nodules and if the distance of the candidate nodule to any nodule is less than 3/2 of the radius of the detected nodule or greater than 2/3 of the radius of the nodule then it is considered as potential nodule, it is marked. If after re-training, it is again detected to be a potential nodule then it is a true positive result else it is a false positive result. Out of 4247 potential nodules only 3571 were classified as true positive results by the DFCNet. The true positive *TP* results detected by CNN was approximately 2984 (83%) while *TP* detected by DFCNet was 3179 (89%). DFCNet outperformed the CNN method. The overall sensitivity of CNN and DFCNet was 74.21% and 80.65%, respectively. The performance evaluation of DFCNet and CNN on different dataset is provided in Table 4.

Table 3
Dataset for training and testing.

Dataset	Total CT-Scans cases	CT Scans containing nodules	Total number of nodules	Total number of slices/ images
LIDC-IDRI database [32]	1018	10,531	2669	244,527
RIDER [33]	46	197	47	15,419
SPIE challenge dataset [38]	70	–	–	22,489
LUNA16 [35]	888	9120	1186	551,065
LungCT-Diagnosis [34]	61	634	121	4682
Shanghai Hospital No. 6 dataset	18	184	24	3794

During the training phase, the training loss ($Loss_T$) decreased as training iteration increase in number, while the validation loss ($Loss_V$) increased and accuracy in turn does not improve significantly before attaining a plateau Fig. 9(a). Using the learning techniques in training the DFCNet resulted in improved performance. Therefore, the validation loss is comparatively low and thus the validation accuracy was improved notably as visible in Fig. 9(b). Optimization is done in order to train the DFCNet to classify the dataset which was not annotated (SPIE Challenge dataset). Random initialization caused the validation loss ($Loss_V$) to be within the range of 0.3–0.75 whereas the training loss ($Loss_T$) was decreased to values approximately equal to zero and thus achieved higher final accuracy than the ($Loss_V$). The Shanghai hospital No.6 dataset, RIDER, SPIE Challenge dataset showed the overfitting issue as the dataset was comparatively smaller. The LIDC-IDR and LUNA16 showed consistently better accuracy of classification. The results show that the proposed system DFCNet has suitable accuracy for both annotated and non-annotated dataset.

The classification of the nodules into four stages was done using the DFCNet, T_4 stage nodules (malignant) average diameter d_{avg} was 17.4 mm and the diameter range was d_{max} 3.6 – d_{min} 29.3 mm. In case of T_3 stage nodules, d_{avg} was 13.1 mm and the diameter range was d_{max} 7.7 mm – d_{min} 26.4 mm whereas d_{avg} of T_2 was 9.56 mm and the diameter range was d_{max} 3.4 mm – d_{min} 15.3 mm. The T_1 (benign nodules) d_{avg} was 4.93 mm and the diameter range was d_{max} 3.6 mm – d_{min} 9.3 mm. The morphological features that were considered during the stage classification of Nodule include the volume, density Hounsfield units (HU) of the nodule, perimeter, area and the energy. Other high-level features like sphericity, texture were added into homogeneity attribute. Apart from these features, DFCNet was trained using the LISS database with nine different classes. Nodule is malignant if there are imaging signs of GGO, L, CV, PI classes while if there is BMP imaging sign then it indicates benign nodule in lung, whereas BMP. The remaining three classes C, OP and AB, can be present both in benign or malignant nodule. Furthermore, different classes of imaging signs can be seen in a single nodule thus the final stage classification is obtained considering all these features as well as these nine classes of imaging signs. Table 5 shows the features for the stage classification of the nodules.

The performance of the DFCNet for the stage classification is done by the help of confusion matrix. Fig. 10 shows the confusion matrix of four stages of cancer classified by DFCNet. Table 6 gives the overall recall and precision of the classification phase. For comparison of the proposed work with the existing work, we randomly sampled 1700 images from the training dataset and used them for testing by the trained fully convolutional neural network. Same dataset was used for network model in [16] trained. Firstly, the features were extracted for the fully connected network layer then the Gaussian Process Regression

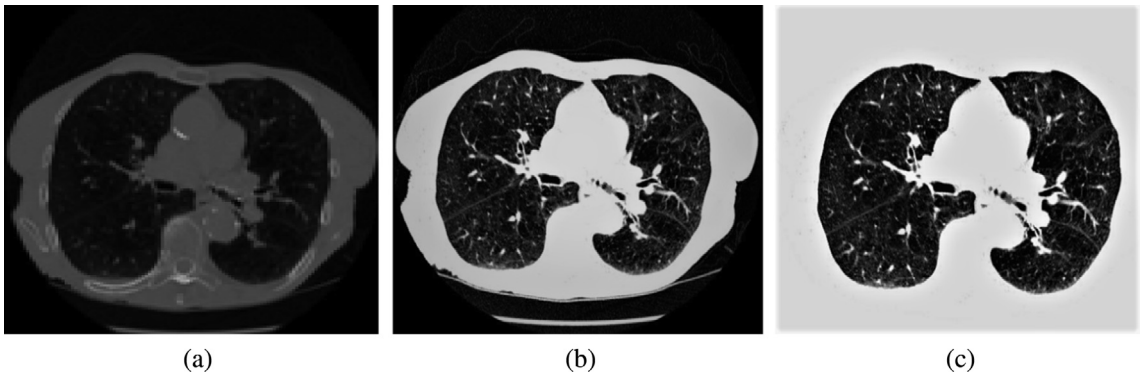

Fig. 7. (a) Original image, (b) image filtered by Gabor, (c) ROI based segmented image.

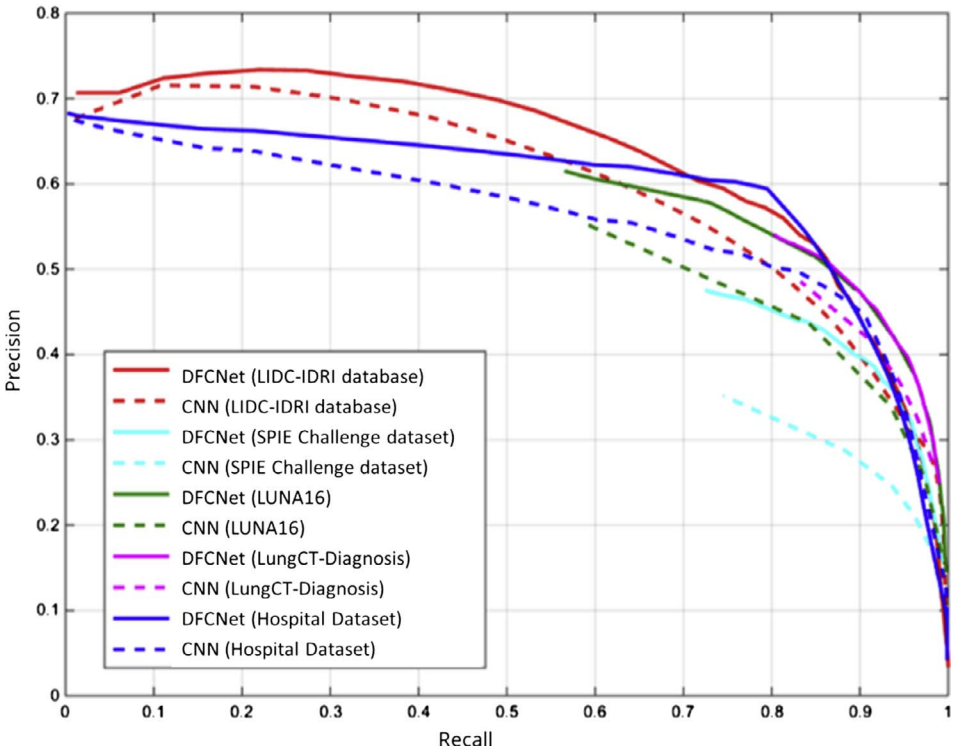

Fig. 8. Performance of DFCNet and CNN on different datasets.

Table 4
Performance evaluation of DFCNet on various dataset.

Dataset	Method	Accuracy (%)	Sensitivity (%)	Specificity (%)	Average false positive
LIDC-IDRI database [32]	CNN	77.61	75.35	80.59	4.4
	DFCNet	86.02	83.91	89.32	2.9
RIDER [33]	CNN	79.22	74.11	81.14	5.5
	DFCNet	80.64	74.58	86.54	3.7
SPIE-Challenge dataset [38]	CNN	73.75	75.65	79.15	4.6
	DFCNet	84.87	81.22	82.97	3.5
LUNA16 [35]	CNN	74.01	70.23	79.47	4.7
	DFCNet	80.12	73.14	81.95	4.2
LungCT-Diagnosis [34]	CNN	81.34	74.71	83.14	2.9
	DFCNet	89.52	82.54	93.60	2.8
Hospital dataset	CNN	79.67	75.23	86.46	2.0
	DFCNet	86.32	83.67	96.17	1.17

Table 5
Extracted features for stage classification.

Features	Stage T_1	Stage T_2	Stage T_3	Stage T_4
Diameter d_{avg}	17.4 mm	23.1 mm	55.56 mm	81.93 mm
Area	206	341	491	608
Perimeter	54.284	77.596	94.52	109.0122
Eccentricity	0.7270	0.6897	0.7909	0.9225
Entropy	0.0092379	0.014346	0.01967	0.023641
Contrast	0.0056	0.0101	0.0131	0.0165
Correlation	0.9271	0.9207	0.9286	0.9275
Energy	0.9983	0.9972	0.9960	0.9950
Homogeneity	0.999	0.998	0.998	0.997

(GPR) was applied to these features. The images were forwarded to the multi-view network to obtain the feature representation and afterward processed by GPR. The results were compared with those obtained by using CNN and Fully convolutional neural network. Table 7 shows the performance comparison of proposed work and TumorNet. The overall accuracy of TumorNet in case of LIDC-IDRI dataset was higher than the accuracy of DFCNet by a factor of 1.39 whereas for the hospital dataset DFCNet and TumorNet accuracies are 96.33 and 81.11, respectively. The main reason behind this improved result of DFCNet was metastasis features for the classification for which different wearable sensors were used. The data collection for the metastasis features was done by using the IoT based personalized health-care systems both clinical system and remote monitoring system. The metastasis feature in addition to the

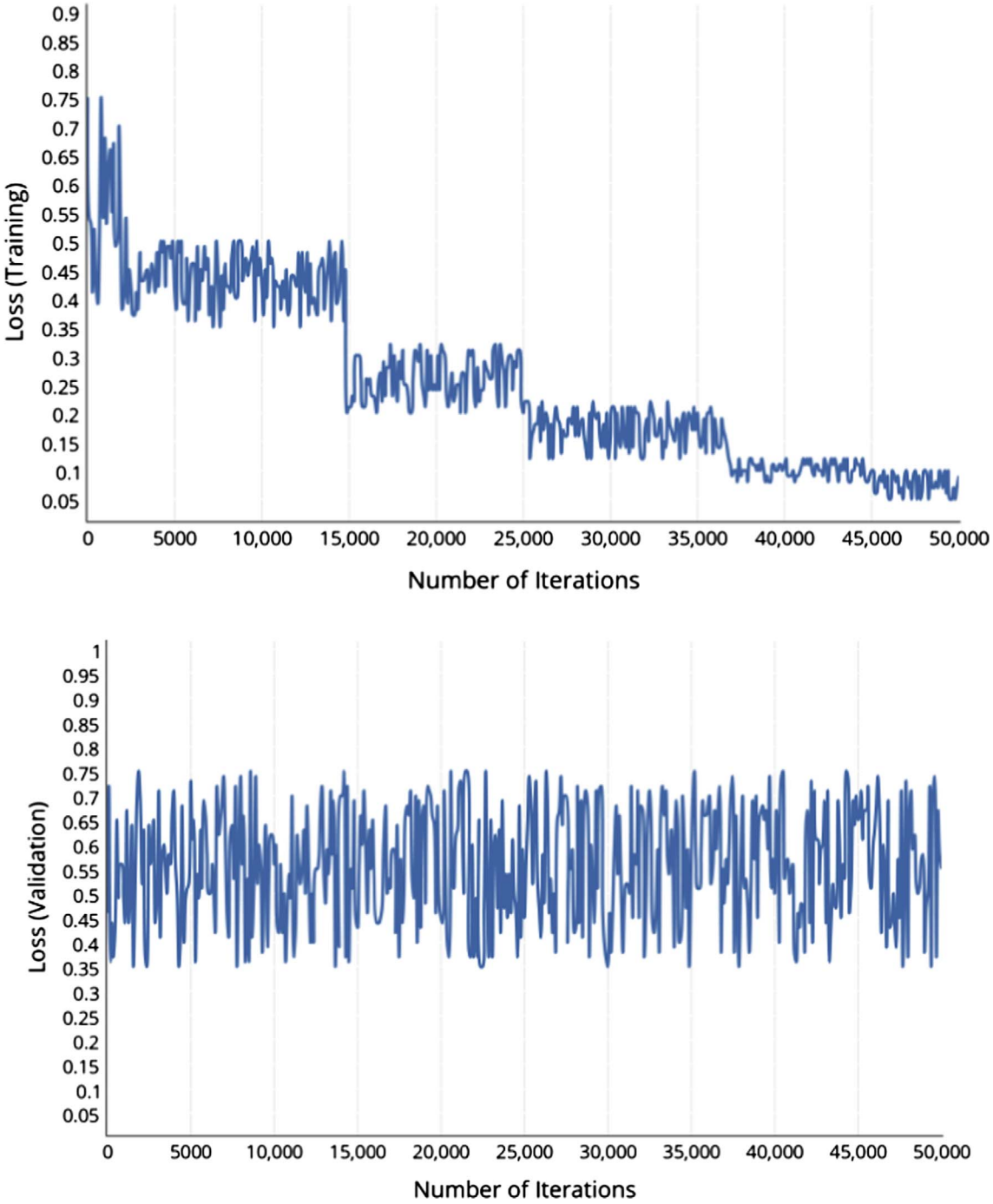

Fig. 9. (a) Training loss ($Loss_T$) vs number of iterations, (b) validation loss ($Loss_V$) vs number of iterations.

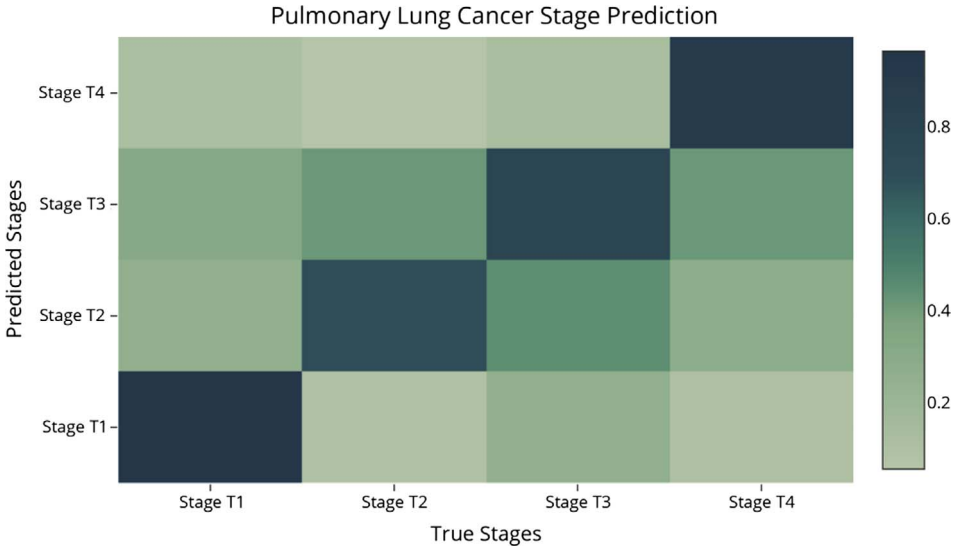

Fig. 10. Confusion matrix for cancer stage classification by DFCNet.

Table 6
Confusion matrix, precision, recall and F-score of stage classification by DFCNet.

Ground truth	Prediction			
	Stage T_1	Stage T_2	Stage T_3	Stage T_4
Stage T_1	0.96	0.08	0.25	0.09
Stage T_2	0.25	0.89	0.44	0.27
Stage T_3	0.31	0.41	0.78	0.41
Stage T_4	0.11	0.05	0.12	0.91
Precision	0.8992	0.7789	0.8221	0.9014
Recall	0.7946	0.7546	0.8148	0.8507
F-score	0.9144	0.8443	0.8596	0.8323

Table 7
Performance comparison of DFCNet and TumorNet.

Dataset	Method	Accuracy (%)	Sensitivity (%)	Specificity (%)
LIDC-IDRI testing dataset	CNN	77.61	75.35	80.59
	DFCNet	86.02	80.91	83.22
	TumorNet	87.41	81.7	85.17
Hospital dataset	CNN	89.67	75.23	86.46
	DFCNet	96.33	83.67	96.17
	TumorNet	81.11	81.49	89.94

training dataset has significant results as compare to TumorNet.

5. Conclusion and future work

One of the benefits of IoT based health care systems is remote access to medical images such as Lung cancer CT-Scan images. IoT services have enabled that the data gathered by the remote machines can also be used for investigating the patterns of the disease and thus disease prediction could be done by using this data for training of CNN. In this paper, we proposed a novel classifier based on deep fully convolutional neural network. DFCNet is a generic classifier which can be used for detection and classification of biomedical images. However, in this paper DFCNet is used to detect and classify the pulmonary nodules in the CT-Scan images. The initial classification was done into two classes i.e. nodule (diseased-Malignant or Benign) and non-nodule (normal). The images classified as nodules are further classified into four lung cancer stages. In order to overcome the problem of limited dataset we used data augmentation techniques. Data augmentation improved the training of DFCNet and enabled it to capture more classification features and learning parameters from enriched training dataset. For the classification of nodule, it was necessary to have equal number of training images in each class, data augmentation techniques were used.

Our method outperformed the existing research work on lung nodule detection. The performance of our proposed method was high even in low-density small-sized pulmonary nodules. The average FP was 3.1 for the DFCNet which was improved to 2.79 using elimination technique. Proposed method used large number of training samples which helped in the improving the performance on the dataset which was not annotated. The limitation of the proposed work is using different dataset with varying scan parameters leading to FP results in case of malignant nodules. Optimal classification results can be obtained if the dataset has same scan parameters. Although using CT-Scan images acquired from varying clinical environment provide more challenging classification for the DFCNet yet improved performance can be achieved using dataset with homogeneous scan parameters. Experimental results and our analysis show that DFCNet achieves better performance than state-of-the-art methods TumorNet. In future, we will focus on using DFCNet for other biomedical images such as MRI for detection and classification of diseases namely breast cancer, brain tumor, colon cancer and diabetic retinopathy. We will detect lung nodule with the proposed method using unseen dataset for testing. Future IoT enabled healthcare methods will be used which aim to provide highly-customized access to rich medical information particularly lung CT images and efficient clinical decision making by the lung cancer CAD system to each individual with unobtrusive and successive sensing and monitoring. The proposed IoT-enabled CAD system could be used for the detection of other types of cancer as DFCNet is a generic method for detection.

Conflict of interest

The authors declare that there is no conflict of interest.

Acknowledgments

The work is supported by the National Natural Science Foundation of China (No. 61572316, 61671290), National High-tech R&D Program of China (863 Program) (No. 2015AA015904), the Key Program for International S&T Cooperation Project (No. 2016YFE0129500) of China, the Science and Technology Commission of Shanghai Municipality (No. 16DZ0501100, 17411952600), the General Program of Cross of Medicine and Engineering of SJTU (YG2015MS19), the interdisciplinary Program of Shanghai Jiao Tong University (No. 14JCY10), a grant from the Research Grants Council of Hong Kong (No.

28200215), and a grant from The Hong Kong Polytechnic University (Project no. 1-ZE8J).

References

[1] J. Qi, P. Yang, M. Hanneghan, S. Tang, Multiple density maps information fusion for effectively assessing intensity pattern of lifelogging physical activity, Neurocomputing 220 (2017) 199–209.

[2] N. Bui, M. Zorzi, Health care applications: a solution based on the internet of things, in: Proceedings of the International Symposium on Applied Sciences in Biomedical and Communication Technologies, 2011, pp. 131:1–131:5.

[3] J. Qi, P. Yang, G. Min, O. Amft, F. Dong, L. Xu, Advanced internet of things for personalised healthcare systems: a survey, Pervasive Mobile Comput. 41 (2017) 132–149.

[4] P. Yang, PRLS-INVES: a general experimental investigation strategy for high accuracy and precision in passive RFID location systems, IEEE Internet Things J. 2 (2) (2015) 159–167.

[5] N.A. Risso, A. Neyem, J.I. Benedetto, M.J. Carrillo, A. Farías, M.J. Gajardo, O. Loyola, A cloud-based mobile system to improve respiratory therapy services at home, J. Biomed. Inform. 63 (2016) 45–53.

[6] S.-J. Lee, Z. Xu, T. Li, Y. Yang, A novel bagging C4.5 algorithm based on wrapper feature selection for supporting wise clinical decision making, J. Biomed. Inform. (2017).

[7] P. Yang, D. Stankevicius, V. Marozas, Z. Deng, E. Liu, A. Lukosevicius, F. Dong, L. Xu, G. Min, Lifelogging data validation model for internet of things enabled personalized healthcare, IEEE Trans. Syst. Man Cybernet.: Syst. (2016).

[8] M. Hassanalieragh, A. Page, T. Soyata, G. Sharma, M. Aktas, G. Mateos, B. Kantarci, S. Andreescu, Health monitoring and management using internet-of-things (IoT) sensing with cloud-based processing: opportunities and challenges, in: Proceedings of the IEEE International Conference on Services Computing, 2015, pp. 285–292.

[9] B. Reeder, A. David, Health at hand: a systematic review of smart watch uses for health and wellness, J. Biomed. Inform. 63 (2016) 269–276.

[10] P. Yang, W. Wu, M. Moniri, C.C. Chibelushi, Efficient object localization using sparsely distributed passive RFID tags, IEEE Trans. Ind. Electron. 60 (12) (2013) 5914–5924.

[11] F. Hu, D. Xie, S. Shen, On the application of the Internet of things in the field of medical and health care, in: Proceedings of the IEEE International Conference on Green Computing and Communications and IEEE Internet of Things and IEEE Cyber, Physical and Social Computing, 2013, pp. 2053–2058.

[12] S.M.R. Islam, D. Kwak, M.H. Kabir, M. Hossain, K.S. Kwak, The Internet of things for health care: a comprehensive survey, IEEE Access 3 (2015) 678–708.

[13] E.J. Topol, S.R. Steinhubl, A. Torkamani, Digital medical tools and sensors, JAMA 313 (4) (2015) 353–354.

[14] K. Ullah, M.A. Shah, S. Zhang, Effective ways to use Internet of things in the field of medical and smart health care, in: Proceedings of the International Conference on Intelligent Systems Engineering, 2016, pp. 372–379.

[15] X. Yan, J. Pang, H. Qi, Y. Zhu, C. Bai, X. Geng, M. Liu, D. Terzopoulos, X. Ding, Classification of lung nodule malignancy risk on computed tomography images using convolutional neural network: a comparison between 2D and 3D strategies, in: C.-S. Chen, J. Lu, K.-K. Ma (Eds.), LNCS 10118, 2016, pp. 91–101.

[16] S. Hussein, R. Gillies, K. Cao, Q. Song, U. Bagci, TumorNet: lung nodule characterization using multi-view convolutional neural network with Gaussian process, in: Proceedings of the IEEE International Symposium on Biomedical Imaging, 2017, pp. 1007–1010.

[17] R. Agarwal, A. Shankhadhar, R.K. Sagar, Detection of lung cancer using content based medical image retrieval, in: Proceedings of the International Conference on Advanced Computing & Communication Technologies, 2015, pp. 48–52.

[18] F. Ciompi, B. de Hoop, S.J. van Riel, K. Chung, E.T. Scholten, M. Oudkerk, P.A. de Jong, M. Prokop, B. van Ginneken, Automatic classification of pulmonary peri-fissural nodules in computed tomography using an ensemble of 2D views and a convolutional neural network out-of-the-box, Med. Image Anal. 26 (1) (2015) 195–202.

[19] A. Teramoto, H. Fujita, O. Yamamuro, T. Tamaki, Automated detection of pulmonary nodules in PET/CT images: ensemble false-positive reduction using a convolutional neural network technique, Med. Phys. 43 (6) (2016) 2821–2827.

[20] J. Chen, J. Chen, H.-Y. Ding, Q.-S. Pan, W.-D. Hong, G. Xu, F.-Y. Yu, Y.-M. Wang, Use of an artificial neural network to construct a model of predicting deep fungal infection in lung cancer patients, Asian Pac. J. Cancer Prev. 16 (12) (2015) 5095–5099.

[21] S. Akram, M.Y. Javed, U. Qamar, A. Khanum, A. Hassan, Artificial neural network based classification of lungs nodule using hybrid features from computerized tomographic images, Appl. Math. Inform. Sci. 9 (1) (2015) 183–195.

[22] A.A. Abdullah, S.M. Shaharum, Lung cancer cell classification method using artificial neural network, Inform. Eng. Lett. 2 (1) (2012) 49–59.

[23] M. Oquab, L. Bottou, I. Laptev, J. Sivic, Learning and transferring mid-level image representations using convolutional neural networks, in: Proceedings of the IEEE Conference on Computer Vision and Pattern Recognition, 2014, pp. 1717–1724.

[24] B. van Ginneken, A.A.A. Setio, C. Jacobs, F. Ciompi, Off-the-shelf convolutional neural network features for pulmonary nodule detection in computed tomography scans, in: Proceedings of the IEEE International Symposium on Biomedical Imaging, 2015, pp. 286–289.

[25] S. Pang, Z. Yu, M.A. Orgun, A novel end-to-end classifier using domain transferred deep convolutional neural networks for biomedical images, Comput. Methods Prog. Biomed. 140 (2017) 283–293.

[26] J. Long, E. Shelhamer, T. Darrell, Fully convolutional networks for semantic segmentation, in: Proceedings of the IEEE Conference on Computer Vision and Pattern Recognition, 2015, pp. 3431–3440.

[27] The American Cancer Society Medical and Editorial Content Team, Signs and Symptoms of Lung Cancer. < http://www.cancer.org/cancer/lung-cancer/prevention-and-early-detection/signs-and-symptoms.html > (accessed 10 October 2017).

[28] S. Quadrelli, G. Lyons, H. Colt, D. Chimondeguy, A. Buero, Clinical characteristics and prognosis of incidentally detected lung cancers, Int. J. Surg. Oncol. 2015 (2015) 287604:1-287604:6.

[29] J.P. Solano, B. Gomes, I.J. Higginson, A comparison of symptom prevalence in far advanced cancer, AIDS, heart disease, chronic obstructive pulmonary disease and renal disease, J. Pain Symptom Manage. 31 (1) (2006) 58–69.

[30] R.C. Bourge, W.T. Abraham, P.B. Adamson, et al., Randomized controlled trial of an implantable continuous hemodynamic monitor in patients with advanced heart failure: the COMPASS-HF study, J. Am. Coll. Cardiol. 51 (11) (2008) 1073–1079.

[31] C. Bhatt, N. Dey, A.S. Ashour (Eds.), Internet of Things and Big Data Technologies for Next Generation Healthcare, Studies in Big Data 23, Springer, 2017.

[32] S.G. Armato III, G. McLennan, L. Bidaut, et al., The lung image database consortium (LIDC) and image database resource initiative (IDRI): a completed reference database of lung nodules on CT scans, Med. Phys. 38 (2) (2011) 915–931.

[33] S.G. Armato III, G. McLennan, C.R. Meyer, A.P. Reeves, M.F. McNitt-Gray, B.Y. Croft, L.P. Clarke, The reference image database to evaluate response to therapy in lung cancer (RIDER) project: a resource for the development of change analysis software, Clin. Pharmacol. Ther. 84 (4) (2016) 448–456.

[34] O. Grove, A.E. Berglund, M.B. Schabath, et al., Data from: quantitative computed tomographic descriptors associate tumor shape complexity and intratumor heterogeneity with prognosis in lung adenocarcinoma, LungCT-Diagnosis Data, Cancer Imag. Arch. (2015), http://dx.doi.org/10.7937/K9/TCIA.2015.A6V7JIWX.

[35] Lung Nodule Analysis Challenge. < http://luna.grand-challenge.org > (accessed 10 October 2017).

[36] K. Clark, B. Vendt, K. Smith, J. Freymann, J. Kirby, P. Koppel, S. Moore, S. Phillips, D. Maffitt, M. Pringle, L. Tarbox, F. Prior, The cancer imaging archive (TCIA): maintaining and operating a public information repository, J. Digit. Imag. 26 (6) (2013) 1045–1057.

[37] G. Han, X. Liu, F. Han, I.N.T. Santika, Y. Zhao, X. Zhao, C. Zhou, The LISS—a public database of common imaging signs of lung diseases for computer-aided detection and diagnosis research and medical education, IEEE Trans. Biomed. Eng. 62 (2) (2015) 648–656.

[38] S.G. Armato III, L. Hadjiiski, G.D. Tourassi, K. Drukker, M.L. Giger, F. Li, G. Redmond, K. Farahani, J.S. Kirby, L.P. Clarke, SPIE-AAPM-NCI lung nodule classification challenge dataset, Cancer Imag. Arch. (2015), http://dx.doi.org/10.7937/K9/TCIA.2015.UZLSU3FL.

[39] A.K. Jain, F. Farrokhnia, Unsupervised texture segmentation using Gabor filters, in: Proceedings of the IEEE International Conference on Systems, Man, and Cybernetics, 1990, pp. 14–19.

[40] K. He, X. Zhang, S. Ren, J. Sun, Delving deep into rectifiers: surpassing human-level performance on ImageNet classification, in: Proceedings of the IEEE International Conference on Computer Vision, 2015, pp. 1026–1034.

[41] A.L. Maas, A.Y. Hannun, A.Y. Ng, Rectifier nonlinearities improve neural network acoustic models, in: Proceedings of the International Conference on Machine Learning, 2013.

[42] W. Liu, Y. Wen, Z. Yu, M. Yang, Large-margin softmax loss for convolutional neural networks, in: Proceedings of the International Conference on Machine Learning, 2016.

[43] S. Ioffe, C. Szegedy, Batch normalization: accelerating deep network training by reducing internal covariate shift, in: Proceedings of the International Conference on Machine Learning, 2015.

[44] J. Duchi, E. Hazan, Y. Singer, Adaptive subgradient methods for online learning and stochastic optimization, J. Mach. Learn. Res. 12 (2011) 2121–2159.

[45] L. Boroczky, L. Zhao, K.P. Lee, Feature subset selection for improving the performance of false positive reduction in lung nodule CAD, IEEE Trans. Inform. Technol. Biomed. 10 (3) (2006) 504–511.